MTL TR 89-104

AD

ROLE OF SHEAR INSTABILITY IN BALLISTIC PENETRATION

JOHN F. MESCALL
U.S. ARMY MATERIALS TECHNOLOGY LABORATORY
MATERIALS DYNAMICS BRANCH

HARRY ROGERS
DREXEL UNIVERSITY
PHILADELPHIA, PA

December 1989

Approved for public release; distribution unlimited.

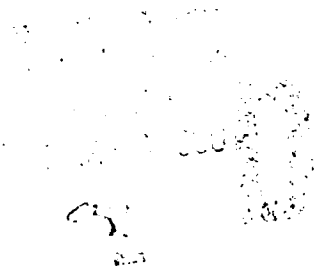

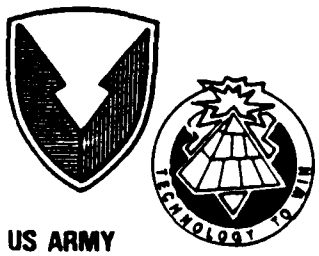

US ARMY
LABORATORY COMMAND
MATERIALS TECHNOLOGY LABORATORY

U.S. ARMY MATERIALS TECHNOLOGY LABORATORY
Watertown, Massachusetts 02172-0001

UNCLASSIFIED

SECURITY CLASSIFICATION OF THIS PAGE *(When Data Entered)*

REPORT DOCUMENTATION PAGE		READ INSTRUCTIONS BEFORE COMPLETING FORM
1. REPORT NUMBER MTL TR 89-104	2. GOVT ACCESSION NO.	3. RECIPIENT'S CATALOG NUMBER
4. TITLE *(and Subtitle)* ROLE OF SHEAR INSTABILITY IN BALLISTIC PENETRATION		5. TYPE OF REPORT & PERIOD COVERED Final Report 6. PERFORMING ORG. REPORT NUMBER
7. AUTHOR(s) John F. Mescall and Harry Rogers*		8. CONTRACT OR GRANT NUMBER(s)
9. PERFORMING ORGANIZATION NAME AND ADDRESS U.S. Army Materials Technology Laboratory Watertown, Massachusetts 02172-0001 SLCMT-MRD		10. PROGRAM ELEMENT, PROJECT, TASK AREA & WORK UNIT NUMBERS
11. CONTROLLING OFFICE NAME AND ADDRESS U.S. Army Laboratory Command 2800 Powder Mill Road Adelphi, Maryland 20783-1145		12. REPORT DATE December 1989 13. NUMBER OF PAGES 27
14. MONITORING AGENCY NAME & ADDRESS *(if different from Controlling Office)*		15. SECURITY CLASS. *(of this report)* Unclassified 15a. DECLASSIFICATION/DOWNGRADING SCHEDULE

16. DISTRIBUTION STATEMENT *(of this Report)*

Approved for public release; distribution unlimited.

17. DISTRIBUTION STATEMENT *(of the abstract entered in Block 20, if different from Report)*

18. SUPPLEMENTARY NOTES

*Drexel University, Philadelphia, PA 19104

19. KEY WORDS *(Continue on reverse side if necessary and identify by block number)*

Adiabatic shear band
Plastic instability
Ballistic penetration
Thermal softening
Work hardening

20. ABSTRACT *(Continue on reverse side if necessary and identify by block number)*

(SEE REVERSE SIDE)

DD FORM 1 JAN 73 1473 EDITION OF 1 NOV 65 IS OBSOLETE

UNCLASSIFIED

SECURITY CLASSIFICATION OF THIS PAGE *(When Data Entered)*

Block No. 20

ABSTRACT

Following a discussion of the role played by adiabatic shear phenomena in ballistic penetration, an experimental procedure is outlined for obtaining quantitive characteristics for specific materials. A computer simulation of the experimental procedure incorporated work-hardening and thermal softening effects and is shown to reproduce experiments in which adiabatic shear bands form, as well as several in which they do not occur. From such supplementary simulations, numerical values for important mechanical properties can be extracted for further application.

CONTENTS

INTRODUCTION

Our objective in this paper is to illustrate the role of adiabatic shear bands in penetration mechanics and to describe an experimental technique by means of which conditions for the incipient nucleation and subsequent growth of such localized bands may be determined. There is abundant experimental evidence to indicate that ballistic results are strongly influenced by the mechanical properties of the materials involved. A particularly instructive example of this is shown in Figure 1 (taken from Reference 1). Two sets of targets were made from the same steel alloy (4340), processed in the same way (VAR) but heat treated to two extremes of strength level, soft (HRC 20) and hard (HRC 52). These targets were of equal thicknesses and were impacted with blunt cylindrical projectiles over a range of velocities. Projectiles were made of the same material as the targets. Their diameters were equal to target thickness and their length was twice their diameter. Recovered targets were cross sectioned and etched.

Comparison of the results shown in Figure 1 reveals that both hard and soft targets fail in what ballisticians term a plugging mode. However, there are interesting differences. The softer target exhibits massive plastic flow and a deep crater forms prior to eventual perforation at a velocity slightly higher than that shown in Figure 1, (2,600 ft/sec). The harder target resists indentation for a much larger range of velocities. There is only a very shallow indentation at an impact velocity of 1,900 ft/sec (Figure 1b). One might easily infer, then, that the velocity required to perforate the harder target would be substantially higher than the 2,600 ft/sec required to perforate the softer one. It turns out, however, that above a critical velocity, an adiabatic shear band (visible in the cross section of the high strength target in Figure 1c) forms in the hard target and leads to "premature" failure at velocities only slightly higher than the value (2,400 ft/sec) shown in Figure 1c. Figure 2 shows the shear band developed in Figure 1 at a high magnification.

This diminished performance is directly attributable to this new mode of failure and illustrates one of the more subtle nuances of the role of material properties in this context. Generally speaking, increased strength or hardness in armor plate leads to increased ballistic performance. To show that the above reversal is not an isolated instance, consider the data shown in Figure 3. A nondimensional measure of ballistic limit is plotted versus Brinell hardness levels for two types of steel with the same chemical composition but processed in two different manners; i.e., vacuum induction melted (VIM) and electroslag remelted (ESR). Targets were one-quarter inch in thickness and all were impacted by similar projectiles. As the target hardness is increased from BHN 250 to approximately BHN 450, target resistance increases dramatically.

Beyond BHN 450, however, target performance drops even faster. Examination of recovered target cross sections reveals three distinct modes of failure: (a) large plastic flow similar to Figure 1a, (b) plugging in a shear mode similar to Figure 1c, and (c) discing which consists of delamination near the target rear surface along planes parallel to the impact face. Figure 3 shows that for both VIM and ESR steels, the drop in ballistic performance is clearly associated with the change in failure mode from plastic flow to shear band formation. Discing is seen only at very high strength levels and leads to even more reduction in performance. It is conjectured that discing is associated with low values of through-thickness toughness. This form of fracture should be distinguished from "spall" which is similar in appearance but is due to the development of large triaxial stress fields upon reflection of the initial compression shock wave from the free rear surface of the target. Peak stresses required to produce spall in steel targets shown in Figure 1 are roughly 30 kbar (450 ksi) which is considerably higher than the static tensile strengths of the steels of Figure 3. The assurance that such stresses are not achieved for the penetration-target interactions of Figure 3, is based on hydrocode simulations of these events (see, for example, Reference 1 and the Appendix).

1. MESCALL, J., and PAPIRNO, R. *Spallation in Cylinder-Plate Impact.* Experimental Mechanics, v. 9, 1974, p. 283-311.

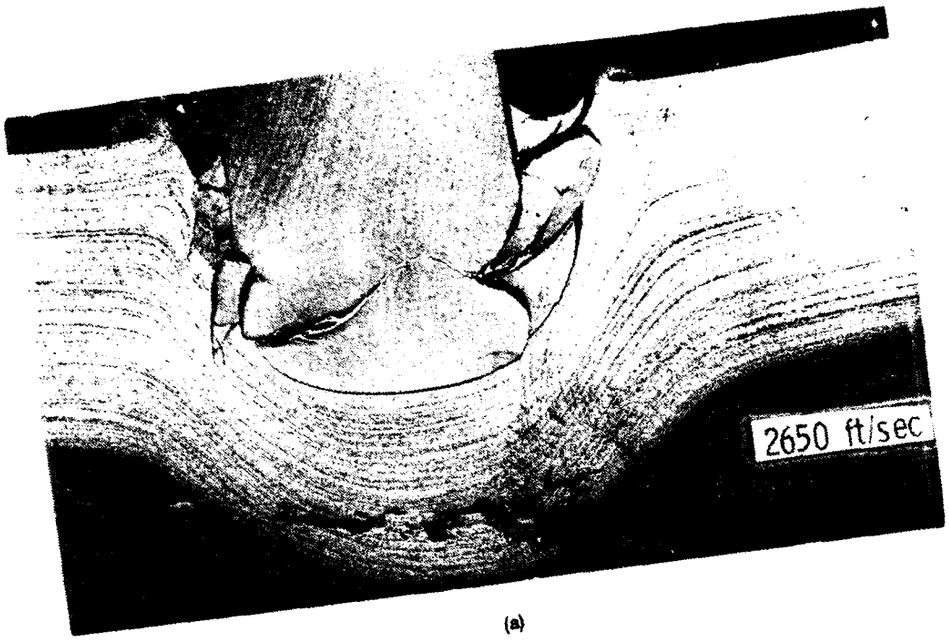

(a)

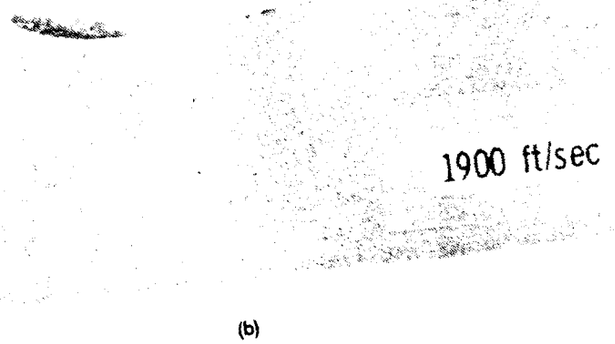

(b)

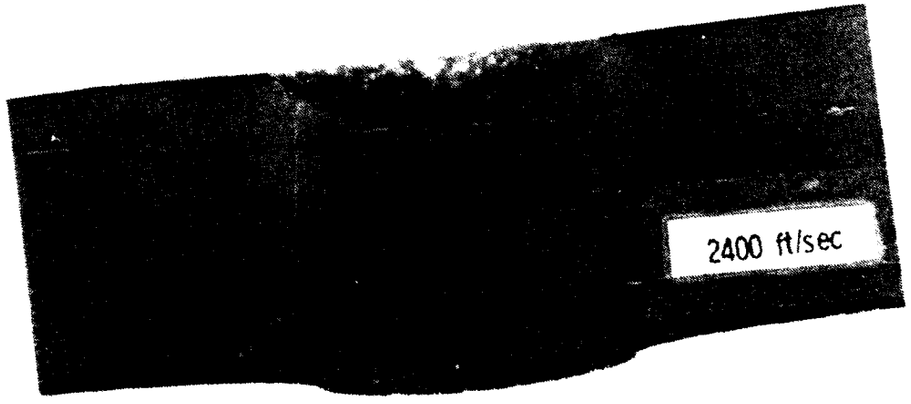

(c)

Figure 1. Cross sections of 4340 steel targets impacted by high strength blunt steel projectiles. Target hardness in (a) is HRC 20. In (b) and (c) hardness is HRC 52. Note differences in crater depth, differences in failure mode, and absence of shear bands in target of (a) and (b).

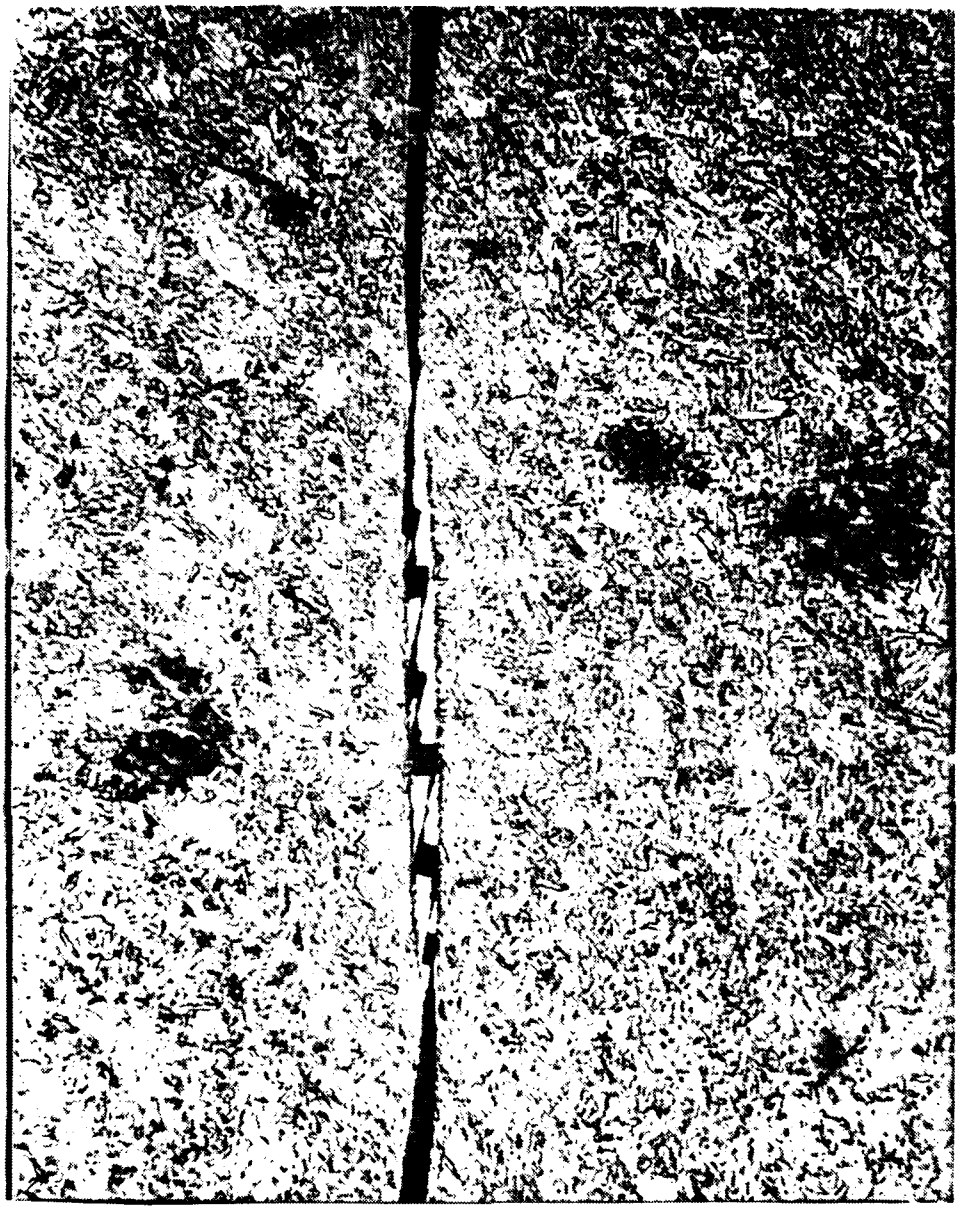

Figure 2. High magnification (500X) of white band of target of Figure 1c.

Clearly then, the material properties most significant for metal targets include dynamic work hardening for the first mode of failure, adiabatic shear onset and growth for the second failure mode, and dynamic toughness in the through-the-thickness sense of discing behavior. We shall address the measurement of the onset of adiabatic shear bands in this paper.

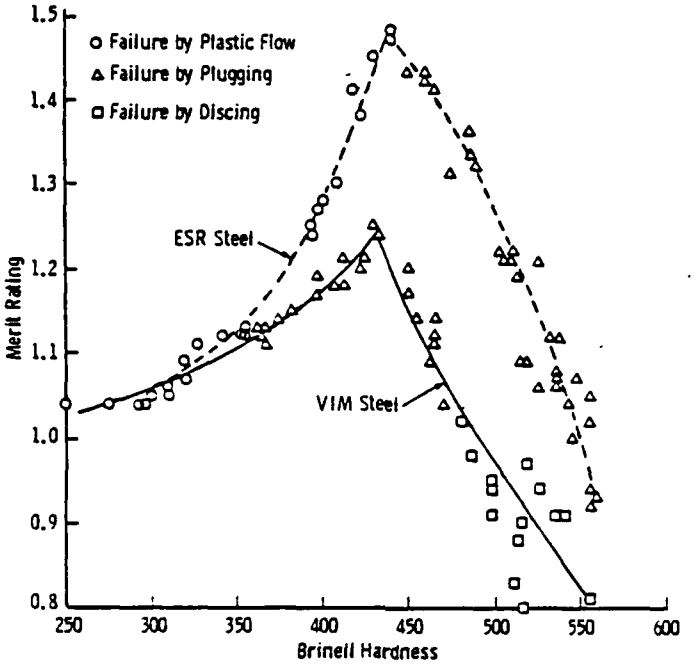

Figure 3. Ballistic merit rating versus hardness for targets of vacuum induction melted (VIM) and electroslag remelted (ESR) steels. Note precipitous decrease in ballistic performance once the failure mode involving adiabatic shear banding is encountered.

CHARACTERISTIC STRESS FIELDS

One of the unspoken difficulties concerning the identification of important material properties in ballistic problems is the fact that both the materials community and a large portion of the mechanics community are relatively unfamiliar with detailed stress and deformation histories experienced in such problems. This is not surprising if one considers the difficulty in obtaining relevant experimental data in a ballistics environment compared with obtaining corresponding data in static laboratory tests.

Perhaps the most obvious remark concerning characteristic stress fields under ballistic conditions is that they are dominated by very large compressive states which are found (by hydrocode computations as in the Appendix) to be divided into a brief initial stage followed by a long steady-state stage and terminated, in many cases, by low order tension fields. The peak stresses in Stage I are found to persist for a few microseconds and to be compressive with peak values on the order of

$$P = V(\rho_1 c_1 \rho_2 c_2)/(\rho_1 c_1 + \rho_2 c_2) \qquad (1)$$

where V is impact velocity, ρ is density, c is sound speed, and P is stress. Convenient/consistent units are cm/μsec, gm/cc, and Mbars. This initial state does not persist for very long because of relief waves which enter from readily available free surfaces on the target impact face. Thus, the stress associated with Equation 1 does not propagate very far into the material, and conditions corresponding to a relatively long steady-state phase soon develop. Associated stress is given by the Bernoulli equation:

$$P = (\rho V^2)/2 \qquad (2)$$

where, again, P is stress, ρ is density, and V is the velocity of the projectile-target interface. Notice that for many impact problems there is close to an order of magnitude difference between Equations 1 and 2. In the example of the Appendix, where a high density penetrator (W or DU) attacks a steel target at a velocity of 0.12 cm/μsec (4,000 ft/sec), peak stresses in Phase I are roughly 350 kbar or 5 million psi; whereas, the peak stress in the steady-state phase is closer to 40 kbar (600,000 psi). The interface velocity V of Equation 2 depends strongly upon the relative impedances (density x sound speed) of projectile and target. However, for materials of the same or similar impedance, it turns out that to a good approximation, V is one-half the impact velocity. It should also be noted that in most ballistic impact problems a local process zone develops immediately in front of the penetrator. This zone moves in time, naturally, however, in spatial extent it is confined to a region roughly one to two projectile diameters in width. Most of the physically interesting processes occur within this process zone; e.g., acceleration and material failure. Unfortunately, this zone is not physically observable and its details must be obtained via computer simulations, such as the Appendix.

MECHANISMS FOR ADIABATIC SHEAR NUCLEATION

The first reported observation of adiabatic shear bands was made by Zener and Holloman (see Reference 2) in 1944. They conjectured that this localization of a shearing process arose because of the deformation-induced temperature rise at rapid rates of loading. Thermal softening, thus, overrode strengthening effects due to strain and strain-rate increases. This is still the conventional view of the process, although an alternative mechanism has recently been put forth by Cowie et al.* Based on the observation that in unconventional shearing tests performed at static and low strain rates (10^2/sec) they observed similar microscopic deformation patterns, they conclude that thermal softening can no longer be considered adominant mechanism since there is adequate time for heat dissipation at static test rates. They propose that a void softening mechanism is operative instead.

However, the character of the large compression field described in the previous section coupled with the short time duration of most ballistic events (tens of microseconds) would seem to vitiate this argument on the role of void formation being a dominant mechanism, at least in ballistic scenarios. Clearly, inclusions may debond or crack under the large imposed shear fields, but the consequence of this would be minimal under the very large, nearly hydrostatic compression fields associated with the process zone. Furthermore, the data obtained by Cowie et. al.* on the dependence of the value of instability strain with pressure also minimizes the possibility of void opening as a mechanism in ballistic events.

We conclude, then, that to describe the initiation of the instability known as adiabatic shear we need to consider the relative roles of work hardening and thermal softening. One could also consider strain-rate hardening effects but a sizeable body of data argues that strain-rate hardening effects are slight compared to strain hardening and thermal softening effects. In Reference 3, we showed that a suitable constitutive formulation which captures the essential features under consideration is given by:

$$Y = Y_o(1 + \alpha\gamma)^n \exp[- \beta T/(T_o - T)] \qquad (3)$$

*COWIE, J. G., AZRIN, M., and OLSON, G. B. Microvoid Formation During Shear Deformation of Ultrahigh Strength Steels. Proceedings of theThirty-Fourth Sagamore Army Materials Research Conference, 1987 (being processed).

2. ZENER, C., and HOLLOMAN, J. Journal of Applied Physics, 15:22, 1944.

3. MESCALL, J. *On the Relative Roles of Strain-Hardening and Thermal-Softening in Adiabatic Shear Bands.* Metallurgical Applications of Shock-Wave and High Strain-Rate Phenomena, Murr, Staudhammer, and Myers, ed., Marcel Dekker, Inc., 1986.

where Y is the flow stress, Y_o is an initial yield stress, γ is the effective plastic strain, α and n are strain hardening parameters, β and T_o are thermal softening parameters, and T, the rise in temperature from some ambient state, is given by:

$$T = \{ \int^{\varepsilon} s_{ij}\, d\varepsilon^{P}_{ij} \} / (\rho c_v) \qquad (4)$$

where ρ is material density, c_v is specific heat, s_{ij} are stress deviators, and ε^{P}_{ij} are plastic strain components.

The flow stress described by Equation 3 is illustrated in Figure 4 for a relatively high strength material (upper curves) and for a relatively low strength material (lower curves). The relative amounts of work hardening (Figure 4a) and thermal softening (Figure 4b) are shown separately. The net combined effects are shown in Figure 4c. We note the presence of a maximum (corresponding to an instability point) for both materials, however, the subsequent decline is precipitous for the high strength material, and more gradual for the lower strength material. When implemented in a finite difference hydrocode such as HEMP or DYNA at each cycle of the explicit numerical integration scheme, one computes the plastic strain and work done at each mesh point and then calculates the corresponding expansion or contraction of the yield circle.

In selecting values for the material parameters associated with thermal softening, the following comments are considered pertinent. Available (static) elevated temperature tests measuring a wide variety of mechanical strength parameters suggest several trends. First, most of the available strength (90%) appears to be depleted by a temperature roughly one-half of the melting temperature. It is unwise, therefore, to choose melting temperature as T_o. Another observation is that the dependence of flow stress on temperature is not well approximated by a linear behavior from ambient to melt as is occasionally done (see Reference 4). For a given alloy, materials which have been processed to a higher strength level exhibit a less stable microstructure and a much more rapid early decline with increasing temperature (Figure 4b, upper); those of intermediate and lower strengths have a more moderate early decline (Figure 4b, lower). After significant temperature increases, there are precipitous drops in strength with the result that these initially separated curves later collapse toward the same low strength value at a common value of temperature, T_o.

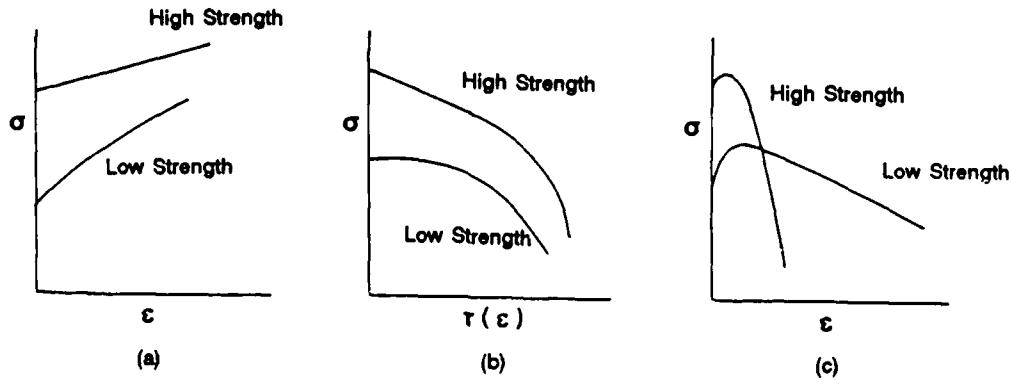

Figure 4. Generic illustration of the dependence of flow stress (a) on strain, (b) on temperature, and (c) on their combined effect. Upper curves refer to high strength steels and lower curves refer to low strength steels.

4. JOHNSON, G., and COOK, W. *Fracture Characteristics of Three Metals Subjected to Various Strains, Strain-Rates, Temperatures and Pressures.* Journal of Engineering Fracture Mechanics, v. 21, no. 1, 1985, p. 31-48.

The question of the influence of time-at-temperature is both important and yet very difficult to assess for the short time involved in high strain-rate applications. We take the point of view here that long-term temperature data serve as useful guides for initial selection of parameters for the model. Improved values can be determined in an interactive process involving comparisons of experimental results with predictions of computer simulations.

No attempt was made to account for thermal flow effects since, for the applications we have in mind, times are too short to permit any significant heat transfer. The issue of strain-rate hardening effects was also not considered since we wished to isolate the thermal effects for now. It is to be emphasized that although strengthening effects due to elevated strain rates are known to be relatively low for rates up to say 100/sec, it is also true that when localized deformation bands develop, strain rate within such bands becomes very high while dropping essentially to zero outside the band. Whether, and by how much, an accounting for this strengthening mechanism in this context would alter perception of events remains to be clarified.

EXPERIMENTAL METHODS

In order to verify and calibrate proposed models of the adiabatic shear band process so that basic metallurgical improvement in armor can be made, it is important that a flexible experimental procedure be available and well understood. Some of the desirable features of such an experimental procedure for the generation and growth of shear bands are that high strain rates be involved, that there be a prevailing hydrostatic pressure field, and that the experiment be amenable to analysis or numerical solution. Some of the existing experimental procedures in vogue are:

- Exploding but constrained cylinders (SRI).
- Torsional Hopkinson bar (Brown University and others).
- Double shear (Charpy) (Cowie/Olson, MTL).
- Stepped projectile impact (Rogers).

Major drawbacks to the exploding cylinder approach are that it is difficult to perform and analyze (thus inhibiting parameter studies), that it is strictly a postmortem examination and, therefore, offers little in the way of studying the nucleation process. The torsional Hopkinson bar experiment also involves postmortem examination, although Duffy has recently generated very interesting photographic observations of the dynamic process; it does not permit generation of shear bands in the presence of large hydrostatic pressure fields. The double shear experiments of Cowie and Olson do not involve high strain rates and are very limited in the level of prevailing hydrostatic pressure imposed.

On the other hand, a very interesting experimental procedure for the study of shear band nucleation and growth is the stepped projectile test in which one impacts a projectile into a small plate of the specimen material to be studied. The projectile is cylindrical in shape and has a blunt cylindrical tip which is embedded into the specimen. Behind the tip and connected to it is a relatively massive cylinder whose shoulders stop further indentation of the projectile tip when they impact the specimen. Rogers (see Reference 5) has demonstrated the flexibility and utility of this approach. He has shown it

5. ROGERS, H. *Adiabatic Shearing — General Nature and Material Aspects* in Material Behavior Under High Stress and Ultra-High Loading Rates, J. Mescall and V. Weiss, ed., New York, Plenum Press, 1983, p 101-118.

is possible to exercise control over the initiation and development of localized bands in a wide class of materials using this procedure. For example, in an annealed 1018 steel impacted at 100 m/sec, the deformation near the corners of the impact crater left by the projectile tip was quite diffuse and showed little tendency to localize. When the same material was cold rolled 67% and impacted at 94 m/sec, a very localized deformation band was found emanating from the corner of the crater. When the latter material was impacted at 100 m/sec, a transformation shear band was found.

We note that this result is consistent with the ballistic observations of Mescall and Papirno (1) who found that when annealed 4340 steel plates were impacted by small, blunt steel cylinders (not stepped projectiles), the penetration process did not involve shear banding in the target. For much higher strength 4340 plates, however, the penetration process was controlled entirely by transformed shear bands (see Figure 1).

There are major differences between the experimental conditions of References 1 and 6 which are of considerable interest. First, although the target thicknesses were nearly the same (0.635 cm), the velocities involved differed by an order of magnitude: 100 m/sec versus 800 m/sec. Next, projectile masses also differed by more than an order of magnitude: 110 grams versus 2 grams. While the kinetic energies of both types of projectiles were, thus, nearly equal, we believe this is not relevant since, as we shall show later, very little of the stepped projectile energy is deposited near the shear bands which develop. Instead, it is transmitted to the support structure.

EXPERIMENTAL RESULTS

The actual experimental arrangement employed to implement the concept of a stepped projectile indentation of steel targets is shown in Figure 5. This "pill and washer" detail is impacted by a blunt cylinder whose diameter is several times that of the pill. Computer simulations of the test setup have been made to demonstrate that this arrangement is fully equivalent to an integral projectile and tip. Naturally, the test setup shown is much more convenient.

A series of experiments were conducted to explore the process of nucleation and growth of adiabatic shear bands in three steels with differing microstructures. Targets were impacted, sectioned, and examined for the presence of shear bands and their length. Figure 6 shows a plot of the length of a shear band developed in a Pearlitic 4140 steel alloy as a function of the depth of penetration (height of pill). Target thickness was 6.35 mm. The four curves of Figure 6 correspond to four values of the backup hole diameter (BHD), as shown in Figure 5. Figures 7 and 8 are corresponding results for 4140 quenched and tempered at 600°C and at 400°C, respectively.

These results clearly indicate a dependence on microstructure. Bands tend to nucleate at much lower values of depth of penetration (smaller initial strain) for the material quenched and tempered at 400°C. Furthermore, the growth of bands in this material is much more rapid, since they traverse target thickness at an indentation level corresponding to that at which bands are just beginning to develop in the other two microstructures. In all cases studied, the rate of growth appeared to be exponential once the band had traversed approximately one-half of the target. Figure 8 shows that the higher strength microstructure (QT at 400°C) was particularly unstable. This is to be expected, however, Figure 8 provides quantitative evidence. Alternatively, the lower strength steels would be expected to resist localization longer because of higher strain hardening rates, smaller flow stress, and smaller temperature rise for a given imposed strain level.

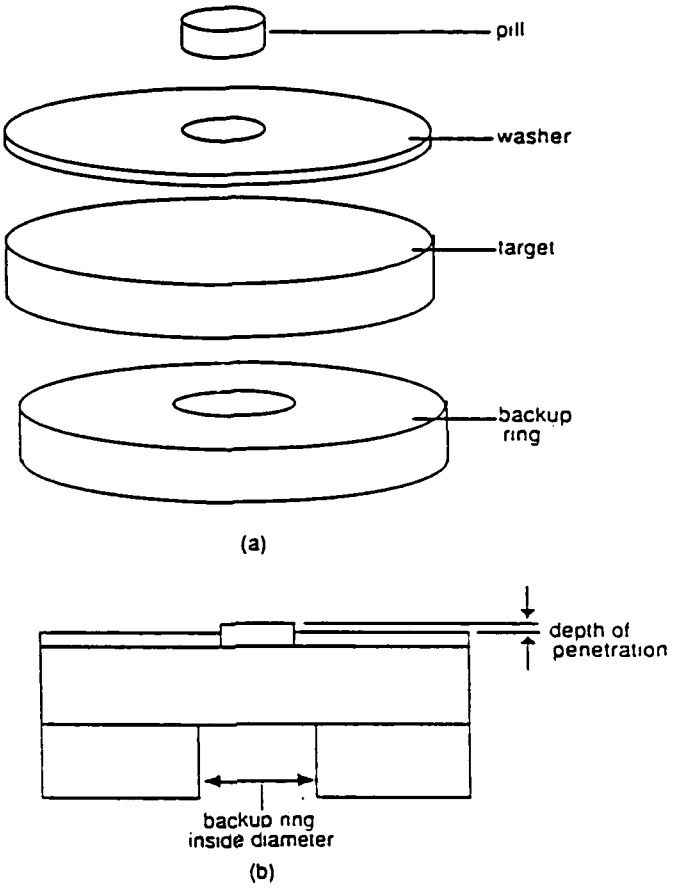

Figure 5. Schematic of details of stepped projectile experiment.

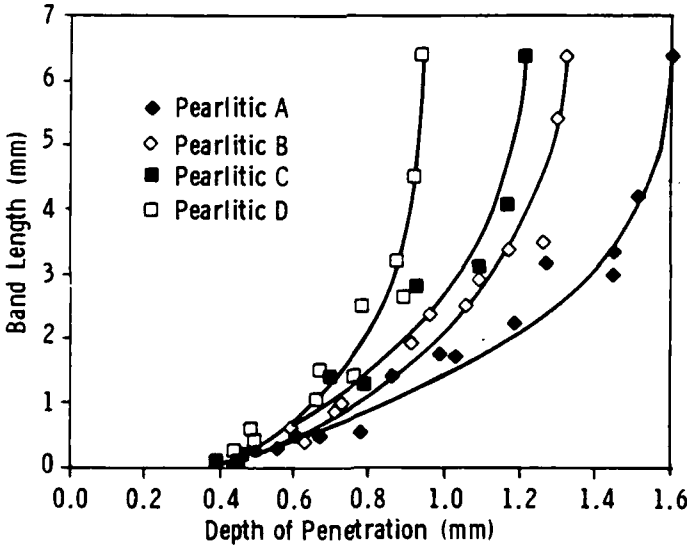

Figure 6. Band length versus depth of penetration for Pearlitic 4140 alloy steel. The letter designation of each plot refers to the backup hole diameter used: A = 1/2", B = 3/8", C = 5/16", and D = 1/4".

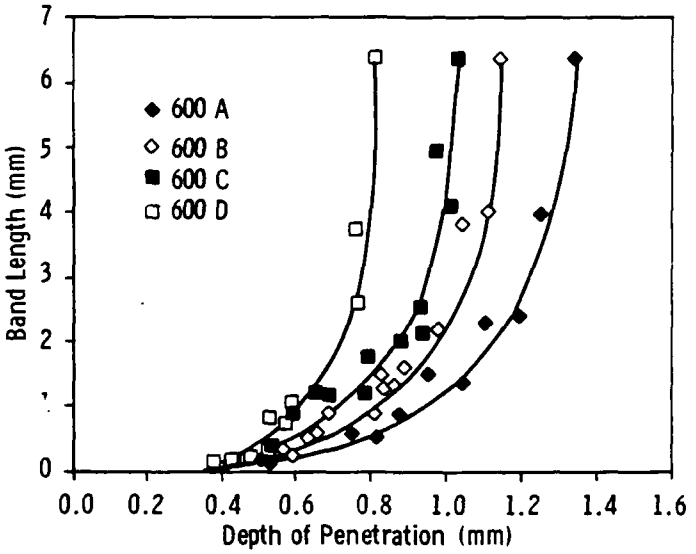

Figure 7. Band length versus depth of penetration for 4140 alloy steel quenched and tempered at 600°C. The letter designation of each plot refers to the backup hole diameter used: A = 1/2", B = 3/8", C = 5/16", and D = 1/4".

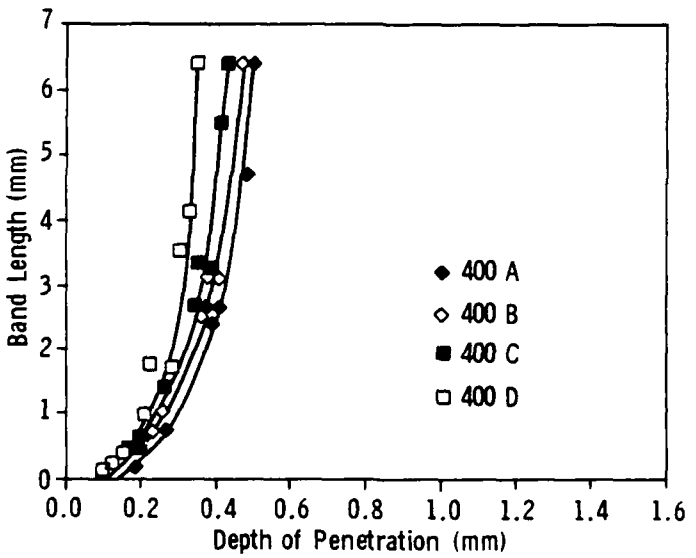

Figure 8. Band length versus depth of penetration for 4140 alloy steel quenched and tempered at 400°C. The letter designation of each plot refers to the backup hold diameter used: A = 1/2", B = 3/8", C = 5/16", and D = 1/4".

Figure 9 (a, b, c, and d) provides a cross plot of the data in which band length is plotted versus depth of penetration for a fixed backup hole diameter. It can be seen that there is a greater dependence on geometry details for the lower strength microstructures than for those quenched and tempered at 400°C.

Finally, Figure 10 shows that bands begin to nucleate within a very narrow variation of impact velocity required for full penetration of the pill.

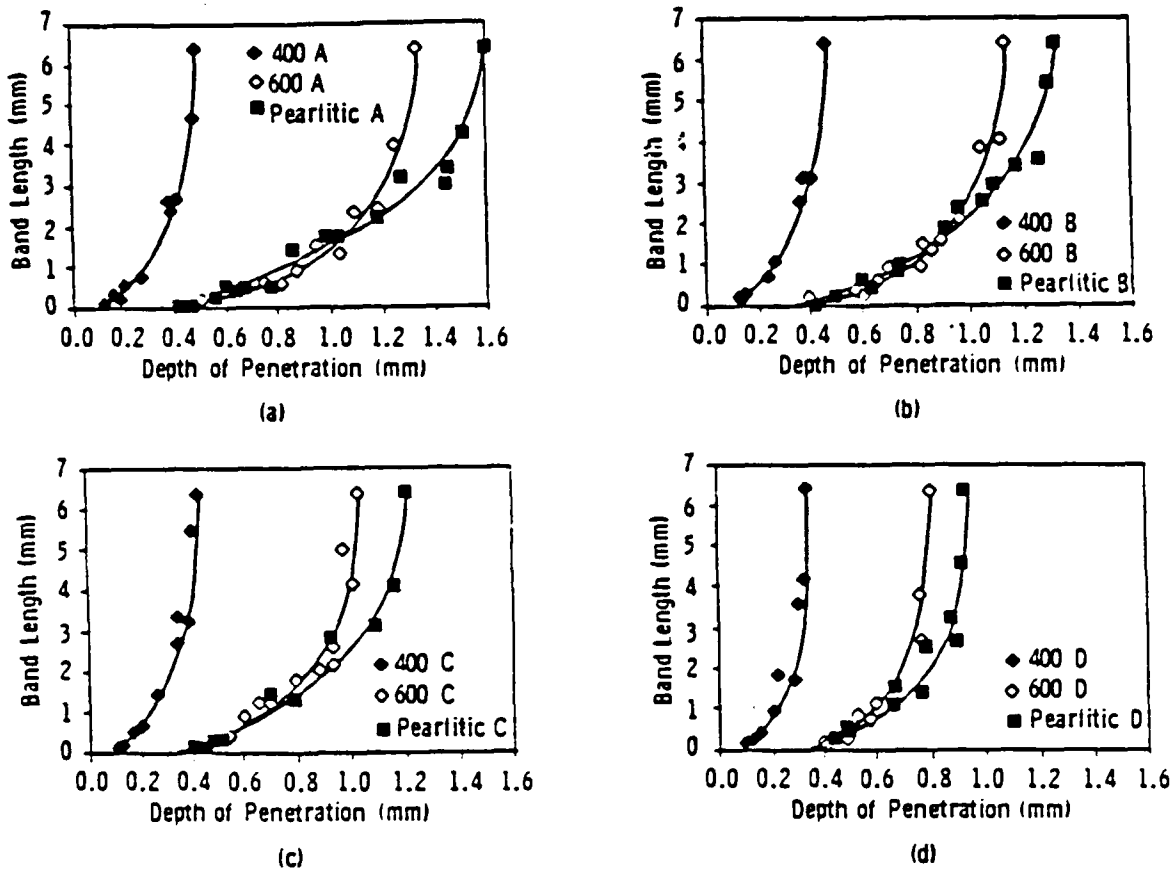

Figure 9. Shear band length versus depth of penetration curves for all three structures of 4140 alloy steel tested for: (a) backup hole diameter "A" (1/2"), (b) backup hole diameter "B" (3/8"), (c) backup hole diameter "C" (5/16"), and (d) backup hole diameter "D" (1/4").

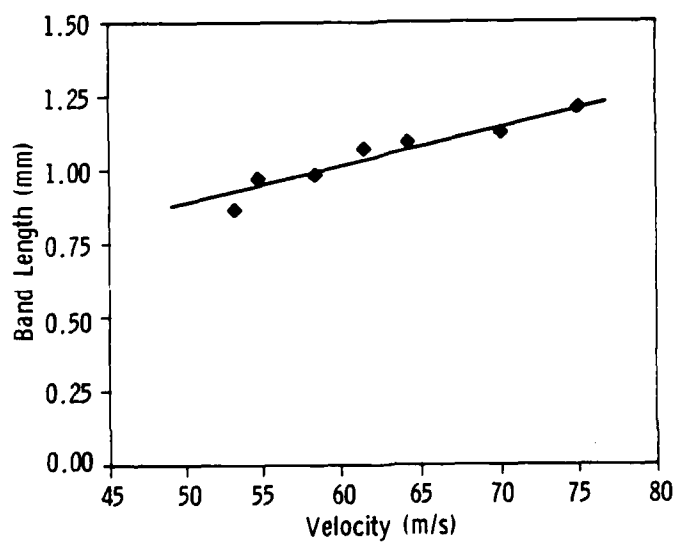

Figure 10. Plot of adiabatic shear band length as a function of projectile impact velocity for Pearlitic 4140 alloy steel targets. A constant backup hole diameter of 1/4" was used.

COMPUTER SIMULATIONS OF STEPPED PROJECTILE EXPERIMENTS

Clearly, computer simulations of the stepped projectile test would serve to make it even more useful by permitting us to obtain results not directly observable in experiments. Our initial objectives were to assess the suitability of the constitutive model described above for predicting the onset of localized deformation in such experiments. Other objectives include the extraction of material parameters from an iterative series of tests and simulations. Some general results (before a discussion of detailed results) include the observation that the rear surface of the target should be rigidly supported outside a small circular region whose center coincides with the axis of the projectile; otherwise, the response of the target to impact involves a large amount of structural bending which influences the deformation interaction between target and tip in an undesirable manner. Another observation, which simplifies the simulation details, is that it is permissible to model only the tip and not the projectile with the stipulation that the velocity of the tip rear surface is held at a constant value until its plane reaches the face of the target. The shoulder portion of the projectile is thus considered to behave as an energy reservoir to maintain the imposed velocity on the tip rear surface. Simulations involving a full description of tip and shoulder indicate that no significant error is introduced by this simplification in the region of interest; i. e., the target-tip interface. Questions might also arise concerning possible modifications of the stress field near the site of potential bands after the shoulder makes contact with the target face. It appears that details of target rear surface support and the low velocities involved (100 to 200 m/sec) combine to render such modifications negligible. The energy stored in the projectile body is primarily absorbed by the support system after the tip is embedded and after the bands are formed if, indeed, they do develop.

Figure 11 presents results for the indentation of a high strength steel target impacted by a stepped projectile (as discussed) at a velocity of 61 m/sec (200 ft/sec). Material properties employed in this example were Y_o = 20 kbar, n = 0.06, α = 12, β = 1.0, and T_o = 660°C (see Equation 1). Backup hole diameter was one-half inch, or twice the projectile diameter. Figure 11a shows the deformation at 15 microseconds after impact. The indentation process has been established; there is slight bulging on the target rear surface but little evidence of strain localization. There is, of course, a highly nonhomogeneous strain field with levels of 100% being obtained near the corners of the rapidly developing crater. Figure 11b presents macroscopic contours of effective plastic strain; contours of 50% and 25% cover an extensive area, however, values of 75% to 100% remain confined to the immediate area of the penetrator corners. Local temperature rises associated with the material properties employed in this specific illustration are only on the order of 400°C, so the thermal softening effect is just beginning to be felt. A very short distance away from the corner zones, strain and temperature levels are quite modest, dropping rapidly to only a few percent or degrees centigrade.

As an aside, we note that the velocity fields developed by this time are ideally suited to develop shear bands in this geometry. The projectile tip maintains an essentially constant velocity. The plug (i.e., the cylindrical region of the target immediately in front of the tip) has been accelerated in a nearly uniform manner to the tip velocity by this time, whereas points outside the plug region are essentially not moving due to the constraints mentioned above. We also note that it is in this context that one finds the greatest differences between the stepped projectile test and the conventional ballistic test. In the latter, one typically fires a smaller projectile at a higher velocity into comparable targets. During the penetration process, the projectile is slowed down considerably and, consequently, details of plug acceleration are quite different. Furthermore, ballistic targets are not supported near the projectile; consequently, the target deformation can be considerably more diffuse.

Figure 11c shows that by 20 microseconds (an indentation of 0.12 cm), localized deformation bands have begun to develop and, in fact, have sufficiently matured so that they reach the rear surface.

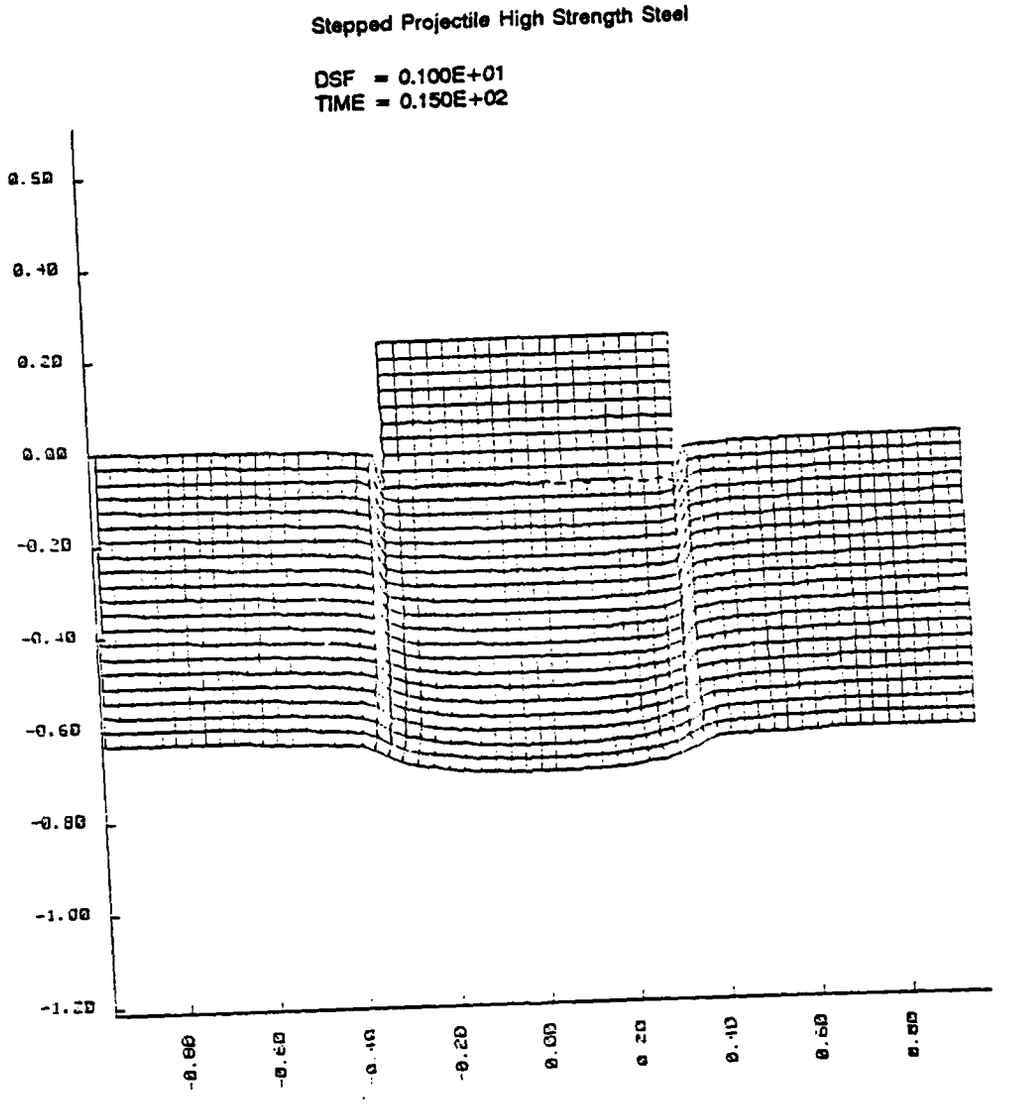

Figure 11a. DYNA simulation of stepped projectile indentation of high strength steel target at 15 microseconds after impact at 200 ft/sec. Backup hole diameter is 1/2" and projectile diameter and target thickness is 1/4".

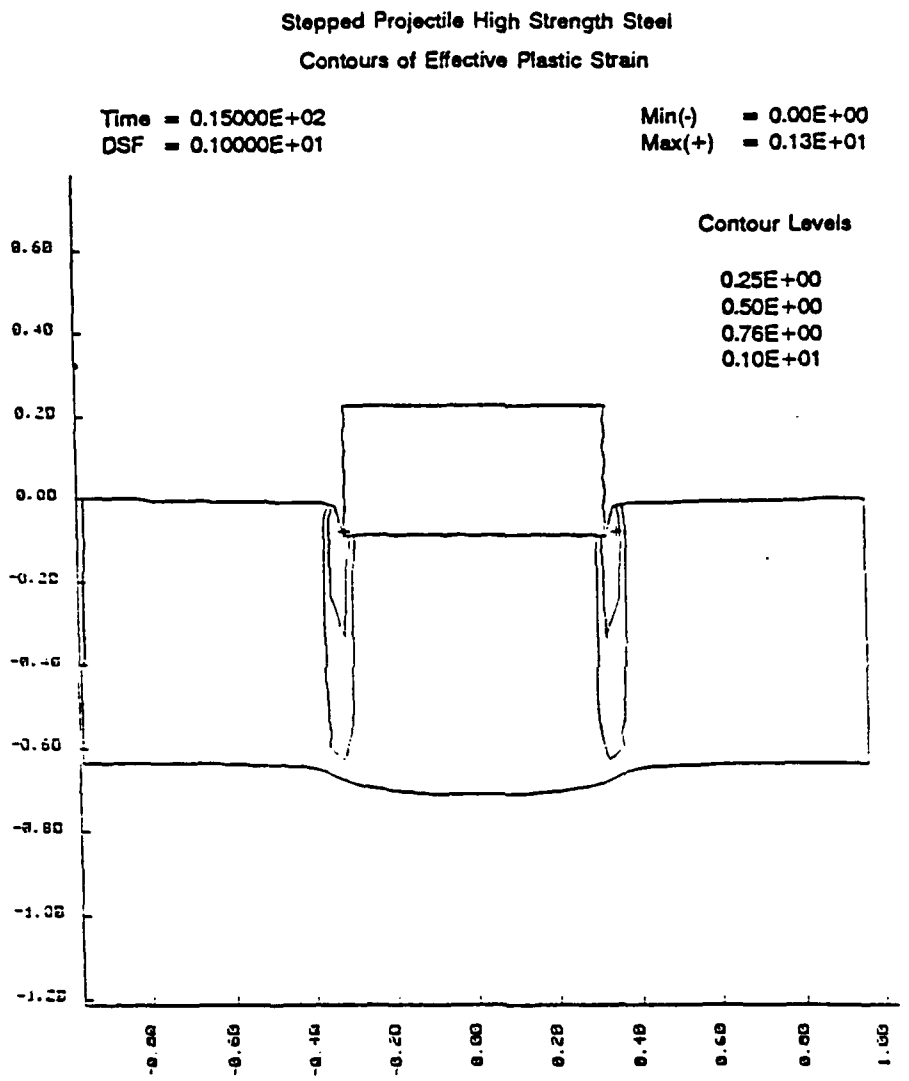

Figure 11b. Effective plastic strain contours (25% and 50%) at 15 microseconds after impact.

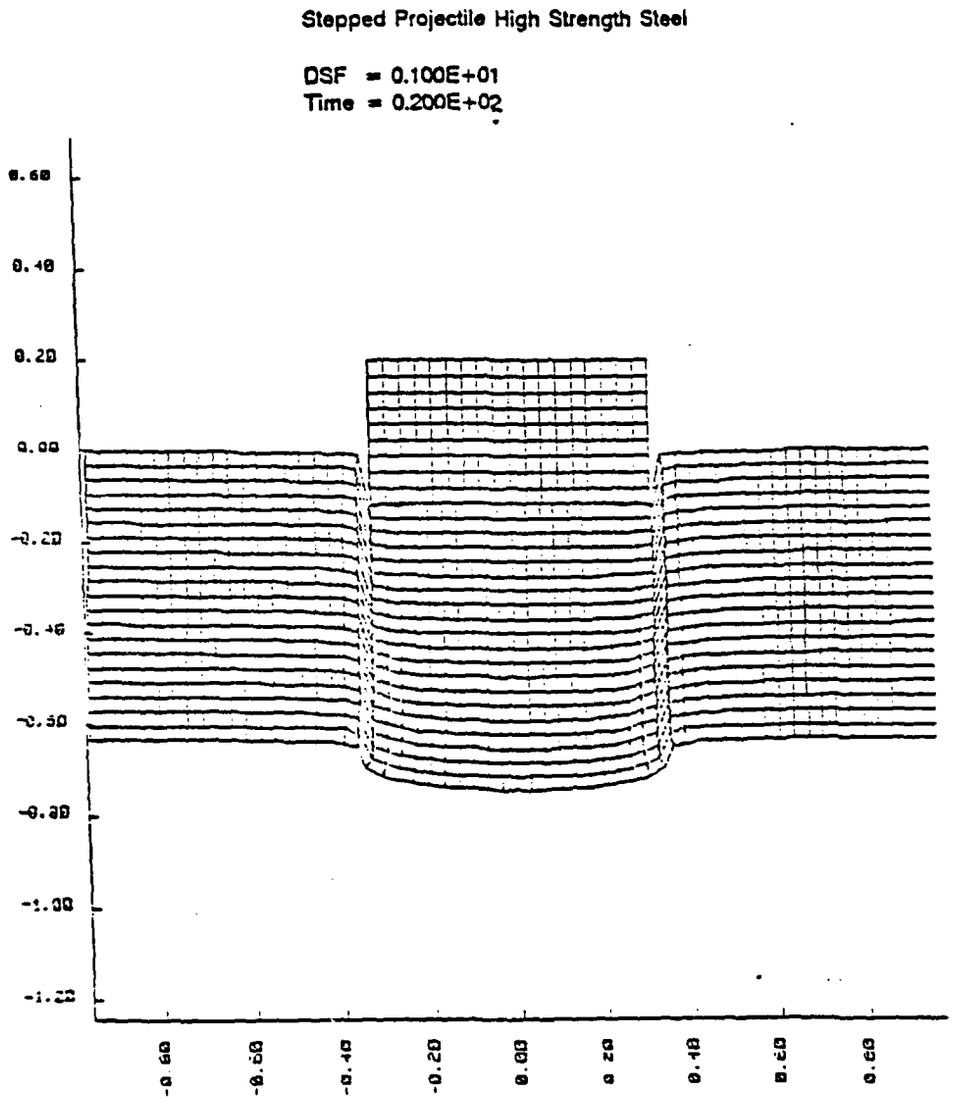

Figure 11c. Indentation of high strength steel projectile at 20 microseconds after impact.

Figure 12 presents results for the impact of a low strength steel target at the same velocity and support conditions as the high strength target of Figure 11. Specific target parameters chosen were Y_o = 0.005 Mbar, n = 0:12, α = 400, β = 1.0, and T_o = 660, thus, the strain hardening rate was increased considerably while the thermal softening rate was the same as in the high strength steel. (In practice, one would expect the initial thermal softening rate to be less than in this numerical example.) Figure 12a shows that the deformation pattern developed in the target is much more diffuse for the softer steel and, at this amount of indentation (0.21 cm), shows little, if any, tendency toward localization. Indeed, the zones immediately in front of the projectile tip have strain hardened and are still above their initial yield stress, having been only mildly softened by the strain-induced temperatures of approximately 150°C. Figure 12b shows the macroscopic contours of effective plastic strain; i. e., 25% and 50%. These cover a significantly smaller volume then do their counterparts for the high strength steel.

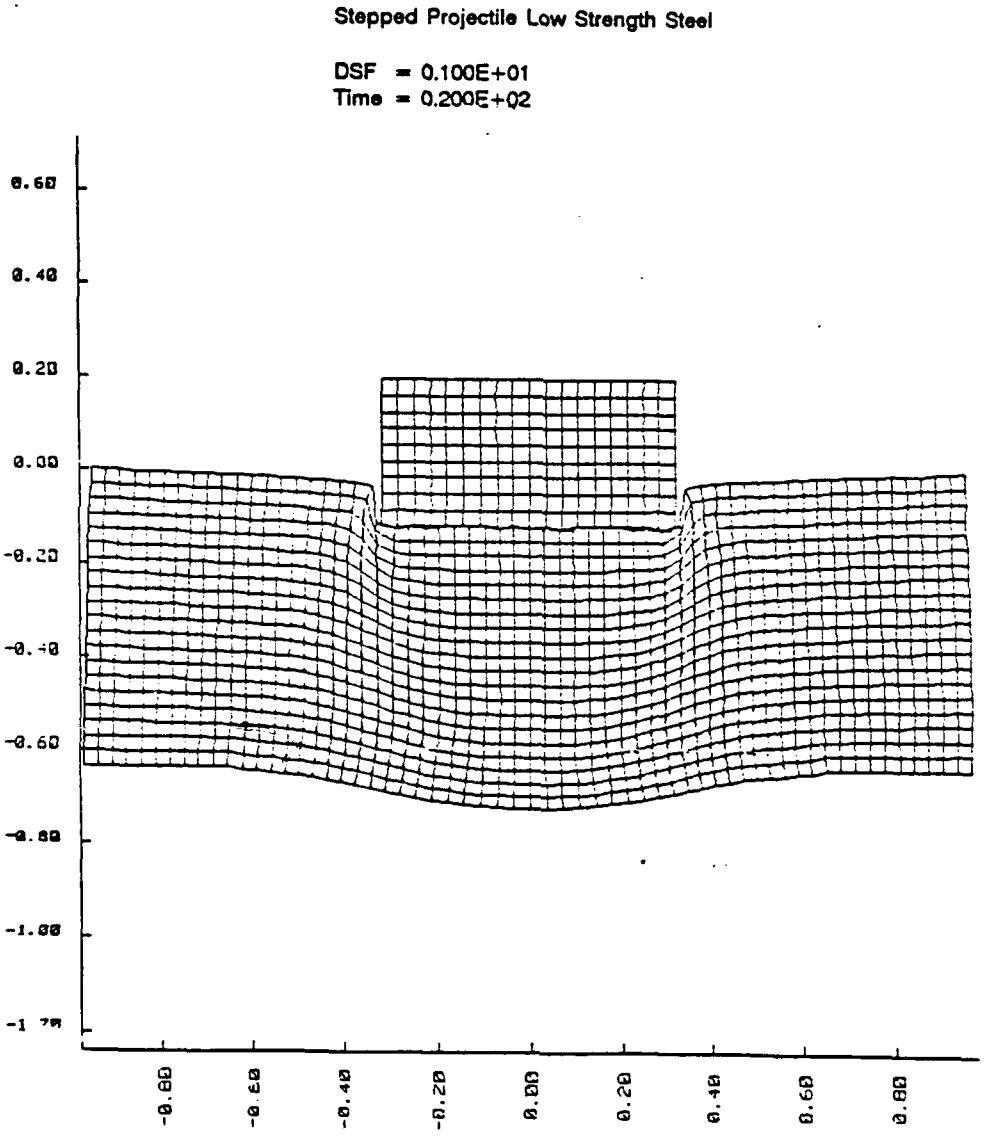

Figure 12a. DYNA simulation of stepped projectile indentation of a soft steel target at 20 microseconds after impact at 200 ft/sec.

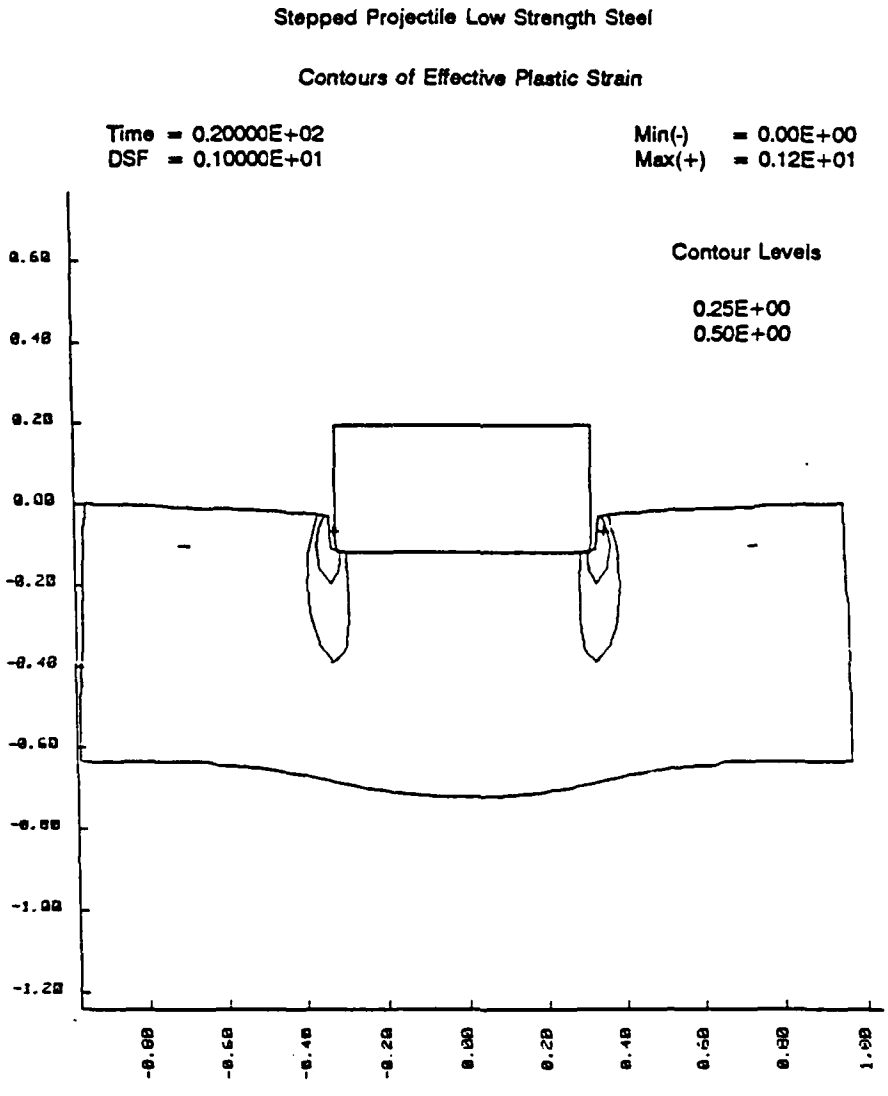

Figure 12b. Contours of effective plastic strain at 20 microseconds after impact of low strength steel target.

Figure 13 presents the stress-strain paths actually followed by each material point for hard and soft steels according to the model of Equation 1.

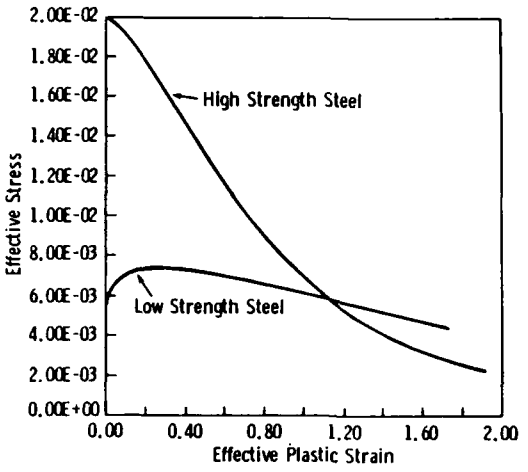

Figure 13. Plot of effective stress in Mbar versus effective strain trajectories followed by high and low strength steel targets of Figures 11 and 12.

The concept of an instability strain (i.e., a maximum in the stress-strain curve) is one which is frequently invoked to characterize a material's sensitivity to shear band formation. Smaller instability strain implies greater sensitivity. The value of the instability strain has little to do, however, with the onset and propagation of shear bands. We find, for example, from our simulations of stepped projectile experiments for high strength steels (Figure 11) that the band which does develop does not mature until the local strain level is much higher than the instability strain. Examination of Figure 11 (a, b, and c) shows that at 15 microseconds after impact, strains greater than 50% have occurred prior to the full development of a mature band, whereas the instability strain is on the order of 5%.

SUMMARY AND DISCUSSION

After discussing the significance of adiabatic shear bands in penetration mechanics, we described the important details of shock waves in ballistic scenarios. We proposed a constitutive relation for work hardening versus thermal softening in the initiation of localized deformations. It appears to us that a proposed role of void nucleation in the formation of shear bands under ballistic conditions is not a tenable one because of the presence of prevailing states of high hydrostatic compressions. Among several candidate techniques for experimental determination of a material's susceptibility to the formation of adiabatic shear bands, we prefer that of the indentation of a stepped projectile because of its inherently greater control and because of the closer proximity of stress states to the ballistic ones. Computer simulations of the latter experiment add considerable supplementary information and can be used in an iterative fashion to extract relevant information on suitable stress-strain behavior, as well as numerical values pertinent to the nucleation event.

APPENDIX

As an example of how computer simulations can be used to provide insight into both kinematic and material property issues associated with penetration mechanics, consider the problem of a long-rod penetrator made of high density material impacting a thick steel target at a velocity of 4,000 ft/sec (2 cm/μsec). Under these conditions, experiments show that penetration of the target takes place primarily by an erosion mechanism in which a deep crater is formed whose diameter is roughly twice the projectile diameter, and within which both projectile and target material flow back toward the impact face. Experimental observations referred to may be either static postmortem examinations of targets or dynamic shadow graphs which provide information on such things as the velocity of a projectile while external to the target, or data on behind-the-armor debris. What is not observable, generally, of course, is detail concerning the interaction of projectile and target at their moving interface within the target. Thus, the specific advantage provided by computer simulations is that they provide quantitative information on internal states of stress and strain which are not obtainable from other sources. Although the simulation we shall discuss concerns a specific ballistic event and mechanism (erosion), nevertheless, many of the characteristics to be detailed below are common to other impact conditions.

Details of the progression of deformation in both target and penetrator are shown (Figures A-1 through A-4) for times 2, 10, 18, and 22 microseconds after impact. Neither the rear of the target (3 cm thick) nor the aft of the penetrator (5 cm long) is visible in these figures which focus on the impact area. From the simulation we find that the interface velocity drops quickly from its "initial" value of 0.12 cm/μsec to a value of 0.07 at 10 μsec and 0.06 at 22 μsec. At this time, points in the penetrator approximately one diameter to the left of the interface are moving with 98% of their initial velocity. Approximately 30% of the rod length has been consumed by the erosion process.

Details of the dynamic stress fields developed by these impact conditions are shown in Figure A-5. We plot values of constant hydrostatic pressure, *neglecting* deviatoric stress components, simply for convenience.

The stress history within both target and projectile can be divided into three phases. There is an initial shock-propagation phase whose local stress levels are extremely high near the impact zone. These are well approximated by Equation 1 of the text. This first phase does not propagate in space and is extremely short in duration (in the present example, about 2 microseconds). The immediate availability of free surfaces on the target impact face and on the outside diameter of the penetrator induces rare faction waves for attenuation of the initial impact stress fields. These relief waves may be clearly traced in the pressure contours of Figure A-5.

Following the first phase, there is a relatively long second phase depending on the projectile length and target thickness. Stresses in this quasi steady-state phase are well approximated by Equation 2. In the present example, stress amplitudes are 40 to 50 kbars. There is, finally, a third stage which is characterized by a lower amplitude stress level which is more oscillating in nature and which corresponds to the first stages of the structural vibration phase of target response.

Another feature of the dynamic stress field associated with penetration, which may be determined by study of these figures, is the existence of a highly localized spatial region, which we have chosen to call a "process zone." Nearly all the events of physical interest occur within the process zone. In the present example, this zone is about one projectile diameter in radius, is centered at the projectile-target interface, and moves with the interface. Once the quasi steady-state second stage of erosion is entered, only elastic waves move away from the process zone. One kinematic consequence of this is that

significant deceleration of projectile and acceleration of target material occurs only within the process zone. Deceleration of projectile does **not** occur uniformly along the projectile by means of the propagation of plane waves down the cylinder axis. Recall that the velocity of projectile material points just outside the process zone at 22 μsec is about 98% of the initial velocity.

The question arises, naturally, about what experimental evidence is available to verify these predictions of the HEMP simulation. Sequential flash x-rays taken while a long rod penetrates a thick target show that the projectile tail still moves with very nearly its launch velocity even though nearly 50% of the projectile front end has been eroded away in the penetration process. Of course, the x-ray shadow graphs provide only the exposed projectile outline and, thus, we are unable to distinguish any velocity gradient along the projectile length. Nor are we able, in general, to "see" the projectile-target interface because it is within the cavity. However, the data on the velocity of the projectile rear surface velocity reveals a smooth behavior rather than one with discrete decrements which would correspond to periodic arrivals of large amplitude planar waves, if indeed such waves traversed the penetrator axis. We, thus, consider this evidence as tending to confirm the HEMP analysis.

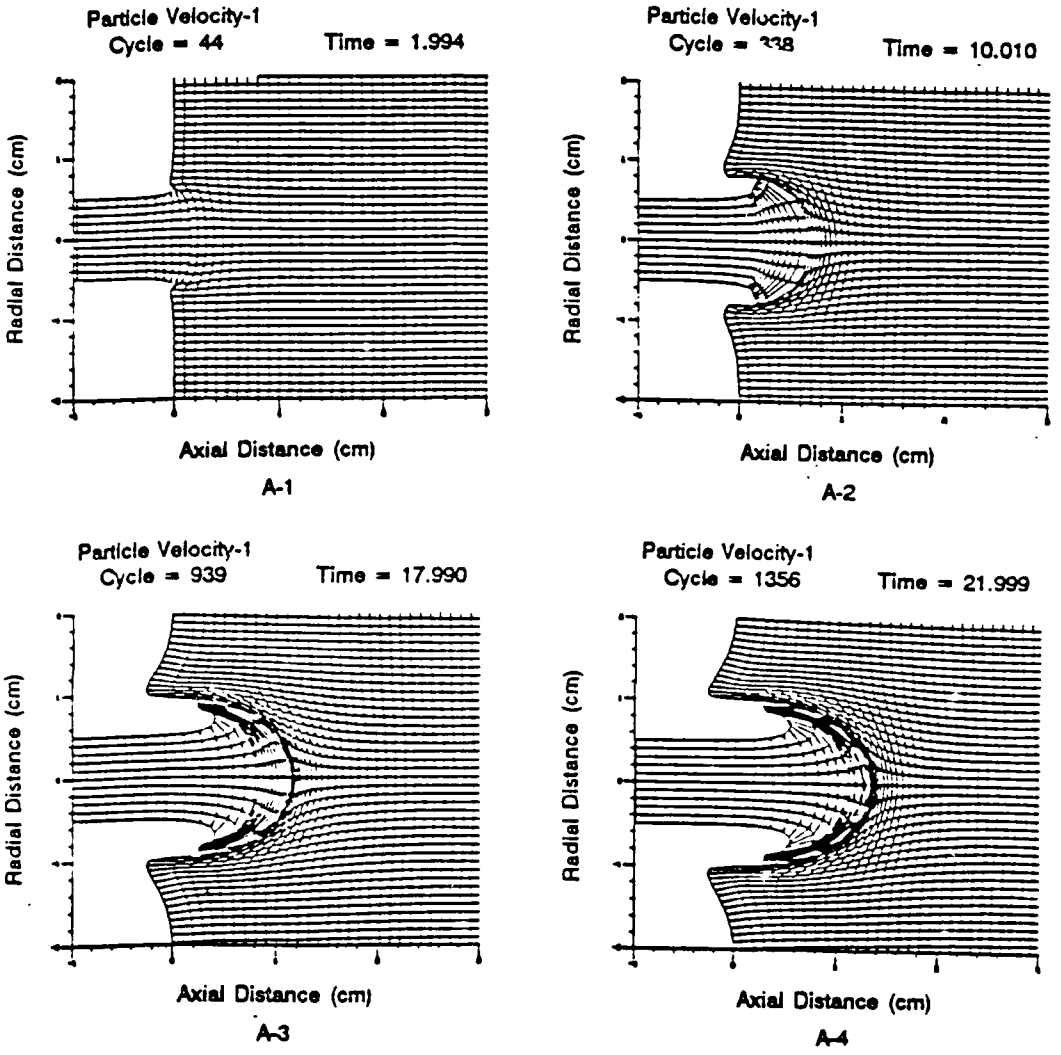

Figures A-1 Through A-4. Computer simulation of penetration of steel target by high density long rod. Impact velocity was 4,000 ft/sec. Figures A-1, A-2, A-3, and A-4 correspond to times 2, 10, 18, and 22 microseconds after impact.

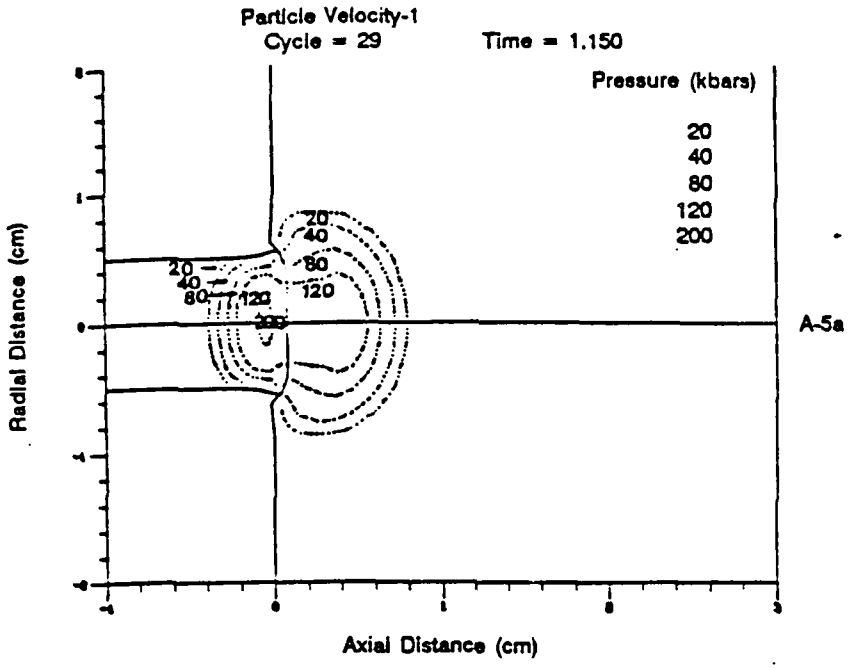

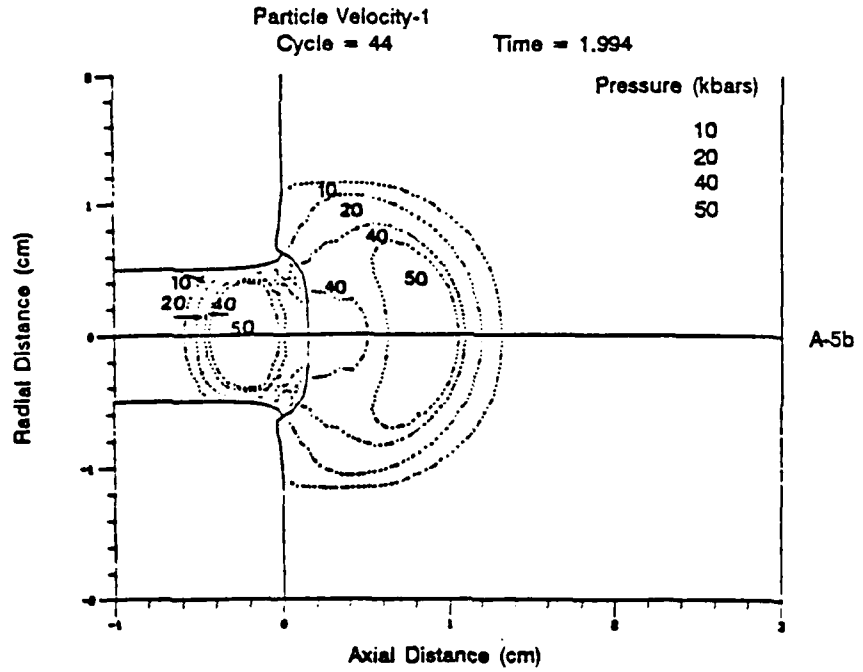

Figures A-5a and A-5b. Isobars of constant pressure (in kilobars) developed as a result of penetration of steel target by high density long rod at 4,000 ft/sec. Approximate times are 1 and 2 microseconds after impact for Figures A-5a and A-5b, respectively.

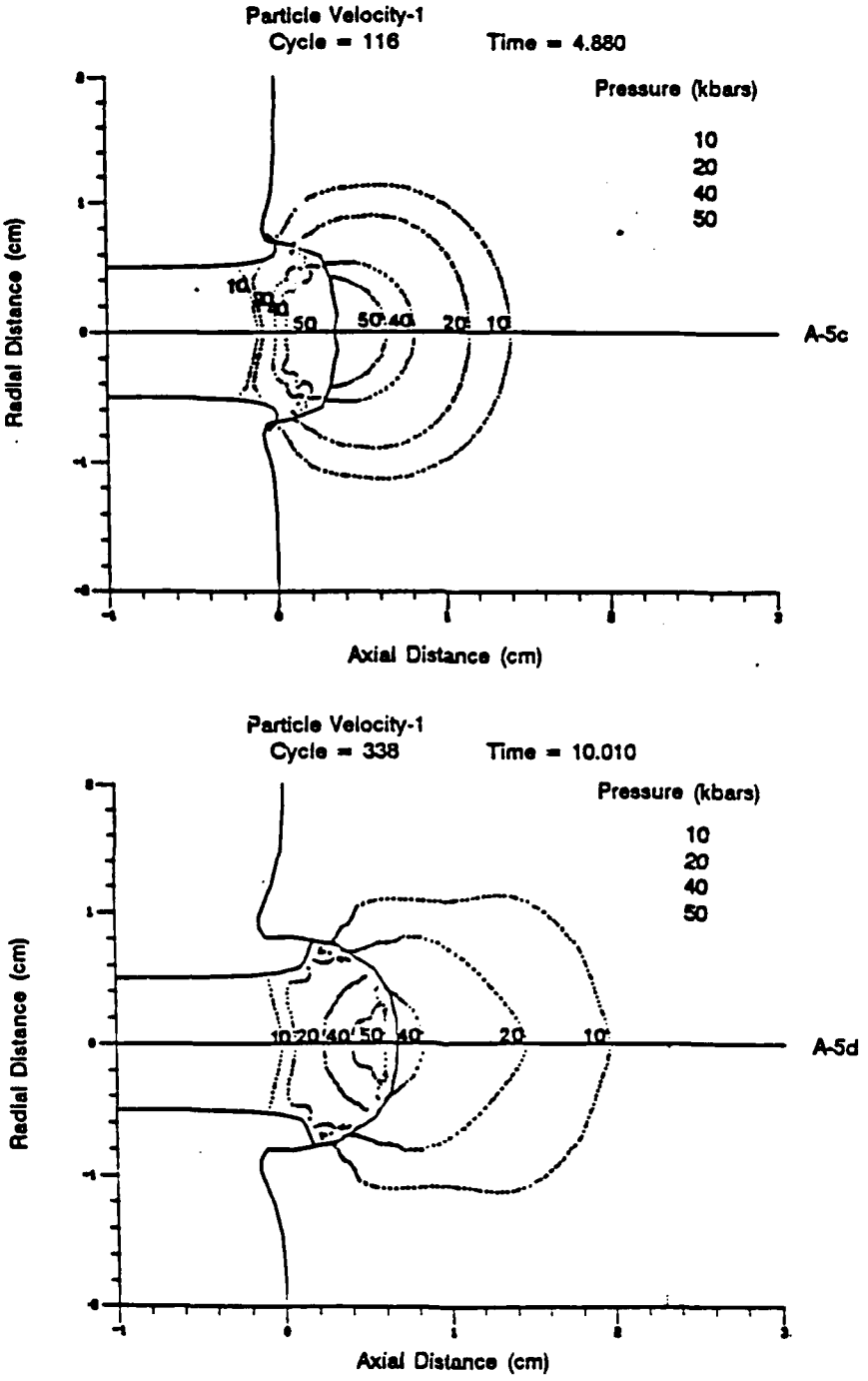

Figures A-5c and A-5d. Isobars of constant pressure (in kilobars) developed as a result of penetration of steel target by high density long rod at 4,000 ft/sec. Approximate times are 5 and 10 microseconds after impact for Figures A-5c and A-5d, respectively.

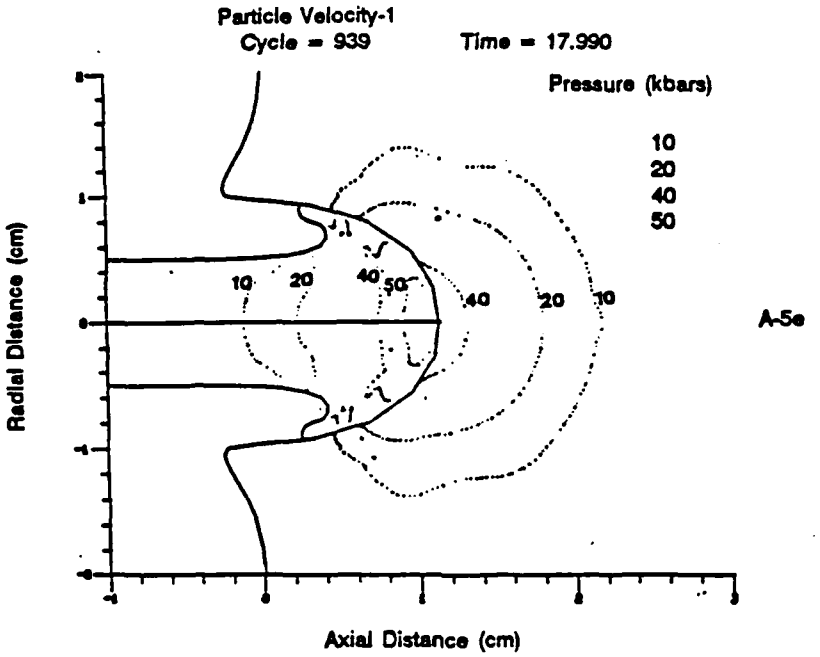

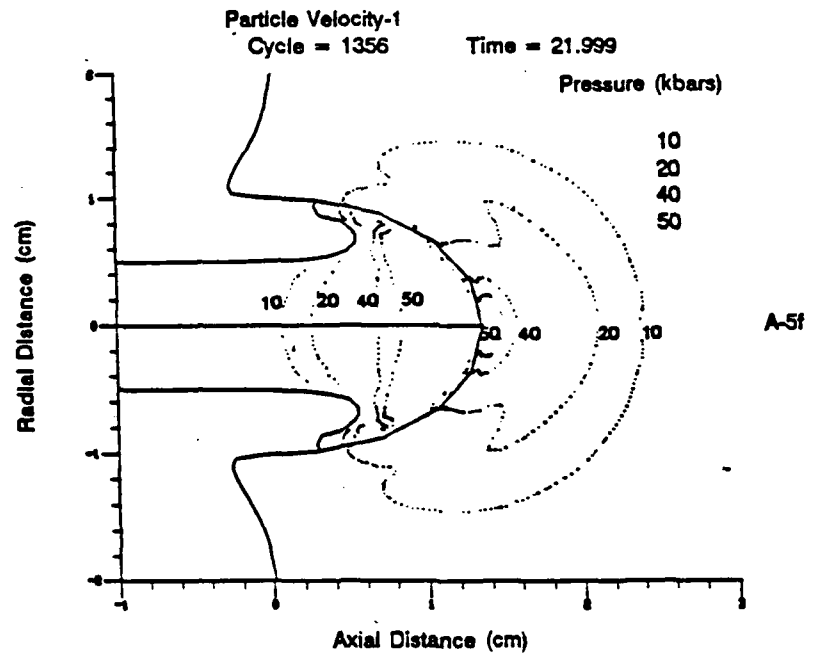

Figures A-5e and A-5f. Isobars of constant pressure (in kilobars) developed as a result of penetration of steel target by high density long rod at 4,000 ft/sec. Approximate times are 18 and 22 microseconds after impact for Figures A-5e and A-5f, respectively.

DISTRIBUTION LIST

No. of Copies	To
1	Office of the Under Secretary of Defense for Research and Engineering, The Pentagon, Washington, DC 20301
	Commander, U.S. Army Laboratory Command, 2800 Powder Mill Road, Adelphi MD 20783-1145
1	ATTN: AMSLC-IM-TL
1	AMSLC-CT
	Commander, Defense Technical Information Center, Cameron Station, Building 5, 5010 Duke Street, Alexandria, VA 22304-6145
2	ATTN: DTIC-FDAC
	Metals and Ceramics Information Center, Battelle Columbus Laboratories, 505 King Avenue, Columbus, OH 43201
1	ATTN: Harry Mindlin
1	Dr. Lee Semiatin
1	E. Hulbert
	Deputy Chief of Staff, Research Development and Acquisition, Headquarters, Department of the Army, Washington, DC 20301
1	ATTN: DAMA-ZE, Mr. C. M. Church
	Commander, Army Research Office, P.O. Box 12211, Research Triangle Park, NC 27709-2211
1	ATTN: Information Processing Office
1	Dr. I. Ahmed
	Commander, U.S. Army Materiel Command, 5001 Eisenhower Avenue, Alexandria, VA 22333
1	ATTN: AMCLD
	Commander, U.S. Army Materiel Systems Analysis Activity, Aberdeen Proving Ground, MD 21005
1	ATTN: AMXSY-MP, H. Cohen
	Commander, U.S. Army Missile Command, Redstone Scientific Information Center, Redstone Arsenal, AL 35809-5241
1	ATTN: AMSMI-RD-CS-R/Doc
	Commander, U.S. Army Armament, Munitions and Chemical Command, Dover, NJ 07801
1	ATTN: Technical Library
1	Dr. J. Beetle
1	Dr. F. Witt
	Commander, U.S. Army Tank-Automotive Command, Warren, MI 48397-5000
1	ATTN: AMSTA-ZSK
1	AMSTA-TSL, Technical Library
	Commander, U.S. Army Foreign Science and Technology Center, 220 7th Street, N.E., Charlottesville, VA 22901
1	ATTN: Military Tech, Mr. Marley
	Commander, U.S. Army Aviation Systems Command, Aviation Research and Technology Activity, Aviation Applied Technology Directorate, Fort Eustis, VA 23604-5577
1	ATTN: SAVDL-E-MOS
	Naval Research Laboratory, Washington, DC 20375
1	ATTN: Code 5830
1	Code 2627
	Chief of Naval Research, Arlington, VA 22217
1	ATTN: Code 471
	Director, Structural Mechanics Research, Office of Naval Research, 800 North Quincy Street, Arlington, VA 22203
1	ATTN: Dr. R. Barsoum
	NASA - Marshall Space Flight Center, Huntsville, AL 35812
1	ATTN: R. J. Schwinghammer, EH01, Dir, M&P Lab
1	Mr. W. A. Wilson, EH41, Bldg. 4612

No. of Copies	To
	Air Force Armament Laboratory, Eglin Air Force Base, FL 32542
1	ATTN: AFATL/DLYA, V. D. Thornton
	Naval Surface Weapons Center, Dahlgren, VA 23448
1	ATTN: W. Mannschreck
1	C. Crowe
	Naval Weapons Center, China Lake, CA 93555
1	ATTN: Mr. M. Bockman
1	Dr. J. Pearson
	Arizona State University, College of Engineering and Applied Sciences, Tempe, AZ 85281
1	ATTN: Prof. Milton C. Shaw
	Denver Research Institute, 2390 South University Boulevard, Denver, CO 80210
1	ATTN: Dr. R. Recht
1	Dr. C. Hoggart
	Drexel University, Dept. of Materials Engineering, Philadelphia, PA 19104
1	ATTN: Prof. Harry C. Rogers
	Drexel University, Dept. of Mechanical Engineering, 32nd and Chestnut Streets, Philadelphia, PA 19104
1	ATTN: Dr. P. C. Chou
1	Dr. R. Toland
	Massachusetts Institute of Technology, Dept. of Mechanical Engineering, Room 1-306, Cambridge, MA 02139
1	ATTN: Prof. Ali S. Argon
	Lawrence Radiation Laboratories, Livermore, CA 94550
1	ATTN: Dr. W. Gourdine
1	Dr. M. Guinan
	University of California, Los Alamos Scientific Laboratory, Los Alamos, NM 87544
1	ATTN: Dr. J. M. Walsh
1	Dr. R. Karpp
1	Dr. E. Cort
	University of Washington, Dept. of Aeronautics and Astronautics, Seattle, WA 98105
1	ATTN: Prof. I. Fyfe
	Stanford Research Institute, 333 Ravenswood Ave., Menlo Park, CA 94025
1	ATTN: Dr. D. Curran
1	Dr. L. Seaman
1	Dr. D. Shockey
	Syracuse University, 304 Administration Building, Syracuse, NY 13210
1	ATTN: Prof. Volker Weiss
	Systems, Science and Software, P.O. Box 1620, La Jolla, CA 92037
1	ATTN: Dr. R. Sedgwick
	Sandia Corporation, Div. 5532, Kirtland Base, East, Albuquerque, NM 87185
1	ATTN: Dr. B. Butcher
1	Dr. A. Stevens
1	Dr. L. Bertholf
1	Dr. D. Grady
1	Dr. M. Kipp
1	Dr. L. Costin
	Southwest Research Institute, 6220 Culebra Road, San Antonio, TX 78248
1	ATTN: Prof. U. Lindholm
1	Dr. C. Anderson
1	Dr. P. Westine
	George Washington University, School of Engineering and Applied Sciences, Washington, DC 20006
1	ATTN: Dr. H. Liebowitz

No. of Copies	To
	Terra Tek, University Research Park, 420 Wakara Way, Salt Lake City, UT 84108
1	ATTN: Mr. S. Green
1	Dr. A. Jones
	Northeastern University, Boston, MA 02115
1	ATTN: Prof. J. N. Rossettos, Dept. of Mech. Eng.
	Tufts University, Medford, MA 02155
1	ATTN: Prof. R. Greif, Dept. of Mech. Eng.
	University of California, Berkeley, CA 94700
1	ATTN: Prof. W. Goldsmith, Dept. of Mech. Eng.
	University of Connecticut, Storrs, CT 06268
1	ATTN: Prof. A. J. McEvilly
	University of Illinois, Champaign, IL 61820
1	ATTN: Prof. D. Drucker, Dean of School of Engineering
	University of Illinois, Urbana, IL 61801
1	ATTN: Prof. T. J. Dolan, Dept. of Theoretical and Applied Mechanics
	University of Pittsburgh, 240 Benedum Hall, Pittsburgh, PA 15261
1	ATTN: Dr. M. L. Williams, Dean of Engineering
	University of Washington, Seattle, WA 98105
1	ATTN: Prof. A. Kobayashi, Dept. of Mech. Eng.
	University of Dayton Research Institute, 300 College Park Avenue, Dayton, OH 45469-0001
1	ATTN: Dr. Steven Bless
	Rockwell International Corporation, Science Center, 1049 Camino Dos Rios, Thousand Oaks, CA 91360
1	ATTN: Dr. Neal E. Paton
1	Dr. Amit K. Ghosh
	Sikorsky Aircraft, A Division of United Aircraft Corporation, Main Street, Stratford, CT 06601
1	ATTN: Mel Schwartz, Chief of Metals
	Teledyne CAE, 1330 Laskey Road, Toledo, OH 43697
1	ATTN: M. Dowdell, Librarian

No. of Copies	To
	Georgia Institute of Technology, Atlanta, GA 30332
1	ATTN: Dr. J. T. Berry, School of Mech. Eng.
	Lukens Steel Company, Coatesville, PA 19320
1	ATTN: Dr. R. S. Swift
	LTV Steel Corporation, 410 Oberlin Avenue SW, Massillon, OH 44646
1	ATTN: Mr. R. Sweeney
1	Mr. W. H. Brechtel
	United States Steel Corporation, Research Laboratory, Monroeville, PA 15146
1	ATTN: Dr. Hsun Hu
	L. Raymond Associates, P.O. Box 7925, Newport Beach, CA 92658-7925
1	ATT: Dr. L. Raymond
	Brown University, Providence, RI 02912
1	ATTN: Prof. J. Duffy, Division of Engineering
	Harvard University, Division of Applied Science, Cambridge, MA 02138
1	ATTN: Prof. B. Budiansky
1	Prof. J. Hutchinson
	Honeywell, Inc., 600 Second Street, N.E., Hopkins, MN 55343
1	ATTN: Mr. Charles R. Hargreaves, Defense Systems Div.
	Director, U.S. Army Ballistic Research Laboratory, Aberdeen Proving Ground, MD 21005
1	ATTN: Dr. J. Frasier
1	Dr. G. L. Filbey
1	Dr. W. Gillich
1	Dr. A. Dietrich
1	Dr. J. Zukas
1	Dr. T. Wright
1	Dr. J. Walker
1	Dr. G. Randers-Pehrson
1	Dr. L. Magness
	Director, U.S. Army Materials Technology Laboratory, Watertown, MA 02172-0001
2	ATTN: SLCMT-TML
2	Authors

U.S. Army Materials Technology Laboratory
Watertown, Massachusetts 02172-0001
ROLE OF SHEAR INSTABILITY IN
BALLISTIC PENETRATION -
John F. Mescall and Harry Rogers

Technical Report MTL TR 89-104, December 1989, 27 pp-
Illustrations

AD_____
UNCLASSIFIED
UNLIMITED DISTRIBUTION

Key Words

Adiabatic shear band
Plastic instability
Ballistic penetration

Following a discussion of the role played by adiabatic shear phenomena in ballistic penetration, an experimental procedure is outlined for obtaining quantitive characteristics for specific materials. A computer simulation of the experimental procedure incorporated work-hardening and thermal softening effects and is shown to reproduce experiments in which adiabatic shear bands form, as well as several in which they do not occur. From such supplementary simulations numerical values for important mechanical properties can be extracted for further application.

U.S. Army Materials Technology Laboratory
Watertown, Massachusetts 02172-0001
ROLE OF SHEAR INSTABILITY IN
BALLISTIC PENETRATION -
John F. Mescall and Harry Rogers

Technical Report MTL TR 89-104, December 1989, 27 pp-
Illustrations

AD_____
UNCLASSIFIED
UNLIMITED DISTRIBUTION

Key Words

Adiabatic shear band
Plastic instability
Ballistic penetration

Following a discussion of the role played by adiabatic shear phenomena in ballistic penetration, an experimental procedure is outlined for obtaining quantitive characteristics for specific materials. A computer simulation of the experimental procedure incorporated work-hardening and thermal softening effects and is shown to reproduce experiments in which adiabatic shear bands form, as well as several in which they do not occur. From such supplementary simulations numerical values for important mechanical properties can be extracted for further application.

U.S. Army Materials Technology Laboratory
Watertown, Massachusetts 02172-0001
ROLE OF SHEAR INSTABILITY IN
BALLISTIC PENETRATION -
John F. Mescall and Harry Rogers

Technical Report MTL TR 89-104, December 1989, 27 pp-
Illustrations

AD_____
UNCLASSIFIED
UNLIMITED DISTRIBUTION

Key Words

Adiabatic shear band
Plastic instability
Ballistic penetration

Following a discussion of the role played by adiabatic shear phenomena in ballistic penetration, an experimental procedure is outlined for obtaining quantitive characteristics for specific materials. A computer simulation of the experimental procedure incorporated work-hardening and thermal softening effects and is shown to reproduce experiments in which adiabatic shear bands form, as well as several in which they do not occur. From such supplementary simulations numerical values for important mechanical properties can be extracted for further application.

U.S. Army Materials Technology Laboratory
Watertown, Massachusetts 02172-0001
ROLE OF SHEAR INSTABILITY IN
BALLISTIC PENETRATION -
John F. Mescall and Harry Rogers

Technical Report MTL TR 89-104, December 1989, 27 pp-
Illustrations

AD_____
UNCLASSIFIED
UNLIMITED DISTRIBUTION

Key Words

Adiabatic shear band
Plastic instability
Ballistic penetration

Following a discussion of the role played by adiabatic shear phenomena in ballistic penetration, an experimental procedure is outlined for obtaining quantitive characteristics for specific materials. A computer simulation of the experimental procedure incorporated work-hardening and thermal softening effects and is shown to reproduce experiments in which adiabatic shear bands form, as well as several in which they do not occur. From such supplementary simulations numerical values for important mechanical properties can be extracted for further application.